AIAA JOURNAL
Vol. 31, No. 9, September 1993

Practical Aspects of Spatially High-Order Accurate Methods

Andrew G. Godfrey,* Curtis R. Mitchell,* and Robert W. Walters†
Virginia Polytechnic Institute and State University, Blacksburg, Virginia 24061

The computational qualities of spatially high-order accurate methods for the finite-volume solution of the Euler equations are presented. Multidimensional reconstruction operators discussed include versions of the k-exact and essentially nonoscillatory (ENO) algorithms. The ENO schemes utilized are the reconstruction-via-primitive-function scheme and a dimensionally split ENO reconstruction. High-order operators are compared in terms of reconstruction and solution accuracy, computational cost, and oscillatory behavior in supersonic flows with shocks. Inherent steady-state convergence difficulties are demonstrated for the implemented adaptive-stencil algorithms. An exact solution to the heat equation is used to determine reconstruction error, and the computational intensity is reflected through operation counts. The standard variable-extrapolation method (MUSCL) is included for comparison. Numerical experiments include the Ringleb flow for numerical accuracy and a shock-reflection problem. A vortex-shock interaction demonstrates the ability of the ENO scheme to excel in simulating unsteady high-frequency flow physics.

I. Introduction

THE domain of high-order accurate numerics has recently been broadened with the development of uniformly accurate essentially nonoscillatory (ENO) schemes for structured rectangular grids by Harten and Osher[1] and Harten et al.[2] Traditional total variation diminishing (TVD) schemes have been used with tremendous success in production-level finite-volume codes. For the total variation to decrease, high-order TVD schemes necessarily reduce to first order at local extrema. Usually, numerical oscillations are controlled by limiters at these extrema. The ENO schemes are a proposed class of numerical algorithms which capture physically relevant high-frequency flow phenomena with a uniform interpolation procedure. The extension of the reconstruction-via-primitive procedure to mesh curvature was accomplished as a doctoral project by Casper.[3] Throughout this paper we assume the use of an adequate Riemann solver. We are principally concerned with the interpolation for the left and right fluid-dynamic states.

An ENO scheme specifies requirements on the reconstruction polynomial which is used for interpolation to the cell faces of a control volume. A general reconstruction polynomial approximates to high-order accuracy an unknown function which generates the cell averages at the current time level. The ENO reconstruction is uniformly accurate, meaning that all of the cell-face interpolations are of the same order of accuracy (i.e., no local reductions in accuracy). Nonoscillatory behavior and uniform accuracy are accomplished in a hyperbolic system only if the stencil of cells used in the reconstruction changes from cell to cell and time level to time level. Additionally, the moving stencil eliminates the necessity for traditional limiters which decrease accuracy at extrema in order to prevent the total variation of the solution from increasing.

ENO schemes choose the "best" cells locally in an asymptotic sense to reconstruct the pointwise solution at a cell interface. In this way ENO incorporates gradient information to match the Taylor series. Obtaining essentially nonoscillatory solutions on unstructured grids in the finite-volume setting is not formally apparent. However, efforts of Barth and Frederickson[4] have succeeded in reconstructing pointwise data with k-exact polynomials on general discretizations applicable to smooth fluid physics. Additionally, Abgrall[5] has designed an algorithm which produces ENO solutions within the finite element formulation.

Although a reconstruction must only satisfy conservation on the cell in question, all of the reconstruction methods discussed in this paper (reconstruction via the primitive function, k exact, dimensionally split ENO, and traditional ϕ-κ MUSCL differencing) satisfy conservation for all of the cells used to obtain the reconstruction. Interpolation algorithms should use reconstruction polynomials which satisfy conservation for not only the main parent cell, but also for all of the supporting cells to get a minimum reconstruction error for a given order of accuracy. The reconstruction that satisfies the mean of all of the cells in the stencil matches the high-order terms in a Taylor series expansion.

In this paper we discuss current reconstruction algorithms and their application to hyperbolic systems of equations using the finite-volume formulation. We will describe and discuss the candidates for uniformly high-order accurate reconstruction methods. To achieve arbitrary high-order accuracy in multidimensions, the reconstruction-via-primitive (RP-ENO) or k-exact method should formally be used. However, these methods are computationally expensive both in terms of calculation and memory. A simple, less rigorous, and less expensive ENO method is described which overlaps two one-dimensional interpolations, giving an improvement to the ϕ-κ formulation used in current production level codes. This is loosely termed dimensionally split ENO (DS-ENO). Because cross-derivative terms are neglected, we stress that this simpler method will achieve at best second-order accuracy, will remain uniformly accurate, is less computational work, and has less reconstruction error in the overlap of a pair of degree-two reconstructions than the overlap of a pair of degree-one reconstructions.

In Sec. II we describe RP-ENO for arbitrary accuracy, k-exact for general grids, and DS-ENO, as well as the reconstructions that the ϕ-κ formulation represents. We demonstrate a method for conserving the mean with k-exact reconstructions and for obtaining the smoothest stencil within general discretizations. Steady-state convergence with adaptive-stencil algorithms will always be difficult to obtain because the chattering stencil subsequently changes the local truncation-error constants on every time step. This is shown for several test case steady-state flows.

In Sec. III we present reconstruction errors of an exact solution to the heat equation on a square grid. Results for

Presented as Paper 92-0054 at the AIAA 30th Aerospace Sciences Meeting, Reno, NV, Jan. 6–9, 1992; received Jan. 27, 1992; revision received Dec. 3, 1992; accepted for publication March 11, 1993.

*Research Assistant, Department of Aerospace and Ocean Engineering. Member AIAA.
†Professor, Department of Aerospace and Ocean Engineering. Associate Fellow AIAA.

RP-ENO, k-exact, DS-ENO, and $\kappa = \frac{1}{3}$ reconstructions are given. The computational accuracy is determined from grid refinement, and operations per grid cell show the CPU intensity of each scheme. Numerical solution error to the Ringleb flow is given in Sec. IV. A shock reflection demonstrates the performance of our k-exact reconstruction to adaptively choose smooth data. Results for the DS-ENO scheme are also presented with a modification to reduce near-wall oscillations. The time history of a strong vortex moving through a normal shock in a diverging section is also presented. Conclusions and recommendations are given in Sec. V.

II. Reconstruction Methods

Consider the starting point of any aerodynamic simulation: the governing equations of fluid motion. In their integral form, the equations are

$$\frac{\partial}{\partial t}\int Q\,\mathrm{d}V + \oint f\cdot\hat{n}\,\mathrm{d}s = 0 \tag{1}$$

If we integrate over a discrete space-time domain $[t^n, t^{n+1}]\times[x_{i-\frac{1}{2}}, x_{i+\frac{1}{2}}]$, the fluid-dynamic equations in Eq. (1) can be written exactly as

$$\frac{\bar{Q}^{n-1}-\bar{Q}^n}{\Delta t} + \frac{\hat{f}_{i+\frac{1}{2}}-\hat{f}_{i-\frac{1}{2}}}{\Delta x} = 0 \tag{2}$$

where

$$\bar{Q}^n \equiv \frac{1}{\Delta x}\int_{x_{i-\frac{1}{2}}}^{x_{i+\frac{1}{2}}} Q(x, t^n)\,\mathrm{d}x \tag{3}$$

and

$$\hat{f}_{i+\frac{1}{2}} \equiv \int_{t^n}^{t^{n+1}} f[Q(x_{i+\frac{1}{2}}, t)]\,\mathrm{d}t \tag{4}$$

Any numerical procedure begins here and follows three distinct steps: 1) reconstruction of the pointwise variable field from the cell-average values defined by Eq. (3) (note that from this point onward, the governing equations of fluid motion are *approximated*); 2) numerical evaluation of the flux in Eq. (4) using the cell-face values and an adequate Riemann solver for the flux; and 3) time evolution of the cell averages using a time-stepping procedure.

We address the reconstruction problem of step 1. With a continuous, smooth function $w(x)$ and a discretized domain, we can calculate the cell averages

$$\bar{w}(x_j) = \frac{1}{\Delta x_j}\int_{x_{j-\frac{1}{2}}}^{x_{j+\frac{1}{2}}} w(\xi)\,\mathrm{d}\xi \tag{5}$$

We are concerned with the inverse problem. Given cell-average data, we want to accurately approximate the function $w(x)$. This process is called reconstruction. We are reconstructing an unknown solution from its known cell averages using a polynomial basis set. We will denote the reconstruction polynomial $R(x;\bar{w})$, which reads: R of x given values of $\bar{w}$.

Essentially Nonoscillatory Reconstruction

The group of cell-average data used to compute a reconstruction is known as the support set or support stencil. If a reconstruction is analytically integrated over the domain of the finite-volume cell and yields the known discrete cell average, the reconstruction is said to satisfy or conserve the mean. So, the solitary goal of a reconstruction polynomial is to satisfy the mean for every cell in the support stencil.

The new twist associated with the essentially nonoscillatory schemes is a nonlinear method for selecting the support stencil. The designers of the ENO schemes have specifically set down three defining conditions for their algorithms.[2,6,7] The three conditions are as follows.

1) At all points where $w(x)$ is smooth, a reconstruction from cell averages must be high-order accurate, or

$$R(x;\bar{w}) = w(x) + \mathcal{O}(h^n) \tag{6}$$

The truncation error $\mathcal{O}(h^n)$ can be written as $e(x)h^n$ and can lose an order of accuracy at a discontinuity.

2) The reconstruction must be conservative in the sense that

$$\bar{R}(x_j;\bar{w}) = \bar{w}_j \tag{7}$$

or

$$\frac{1}{\Delta x_j}\int_{x_{j-\frac{1}{2}}}^{x_{j+\frac{1}{2}}} R(\xi;\bar{w})\,\mathrm{d}\xi = \bar{w}(x_j) \tag{8}$$

This means that the reconstruction itself must satisfy the same cell average as the original function.

3) The reconstruction must be essentially nonoscillatory, which in terms of the total variation (TV) means

$$\mathrm{TV}[R(x;\bar{w})] \le \mathrm{TV}[w(x)] + \mathcal{O}(h^n) \tag{9}$$

This simply states that oscillations are allowed only on the level of the truncation error. Arbitrary accuracy and elimination of $\mathcal{O}(1)$ oscillations around discontinuities are achieved at the expense of a slightly increasing total variation.

Primitive Function

Given cell averages $\bar{w}_j$ of a piecewise smooth function $w(x)$ we can immediately evaluate discrete values of the primitive function, denoted $W(x)$. The analytic form is defined starting from an arbitrary point j_0 as

$$W(x) \equiv \int_{x_{j_0-\frac{1}{2}}}^{x} w(\xi)\,\mathrm{d}\xi \tag{10}$$

The discrete values follow from a summation

$$W(x_{j+\frac{1}{2}}) = \sum_{i=j_0}^{j}\Delta x_i\bar{w}_i \tag{11}$$

The desired reconstructed function $w(x)$ is the derivative of the analytic primitive function, or

$$w(x) = \frac{\mathrm{d}W}{\mathrm{d}x} \tag{12}$$

We can apply a Lagrange interpolation polynomial to the discrete values of the primitive function and obtain an ENO interpolation polynomial if we use the "smoothest" stencil. We can then determine an approximation to $w(x)$, which we call $R(x;\bar{w})$, by differentiating the Lagrange polynomial. This procedure conserves the mean and does not require uniformity of the mesh. Note that the primitive function $W(x)$ is by one derivative smoother than $w(x)$.

The primitive function is particularly useful in determining the truncation error of a reconstruction from cell averages. For example, the cell average is a second-order approximation to the function that generated that cell average at the cell centroid. The Taylor series expansion of $W(x_{j+\frac{1}{2}})$ about an arbitrary point x is

$$W(x_{j+\frac{1}{2}}) = W(x) + \frac{\mathrm{d}W}{\mathrm{d}x}(x_{j+\frac{1}{2}}-x) + \sum_{n=2}^{\infty}\frac{\mathrm{d}^nW}{\mathrm{d}x^n}\frac{(x_{j+\frac{1}{2}}-x)^n}{n!} \tag{13}$$

From the definition of the primitive function, we can immediately see that

$$\frac{W(x_{j+\frac{1}{2}})-W(x_{j-\frac{1}{2}})}{\Delta x} = \bar{w}_j \tag{14}$$

Defining $\xi = x - x_j$ and noting that $w(x) = \mathrm{d}W/\mathrm{d}x$, we obtain

$$\bar{w}_j = w(x) + \frac{\mathrm{d}^2W}{\mathrm{d}x^2}\frac{(\xi-\Delta x/2)^2-(\xi+\Delta x/2)^2}{2\Delta x} + \sum_{n=3}^{\infty}\frac{\mathrm{d}^nW}{\mathrm{d}x^n}\frac{(-1)^n[(\xi-\Delta x/2)^n-(\xi+\Delta x/2)^n]}{n!\Delta x} \tag{15}$$

So, at $\xi = 0$, the cell average is a second-order approximation to $w(x)$ at $x = x_j$. The truncation error for higher order reconstructions can be determined similarly.

Essentially Nonoscillatory Definition of Smoothness

An ENO algorithm chooses the "best" stencil in a very nonlinear fashion. The smoothness of the discrete data $W(x_{j+\frac{1}{2}})$ is determined with a divided difference table. If $W(x)$ is $C^n[x_{j+\frac{1}{2}}, x_{j+\frac{1}{2}+n}]$, then

$$W[x_{j+\frac{1}{2}}, x_{j+3/2}, \ldots, x_{j+\frac{1}{2}+n}] = \frac{1}{n!} W^{(n)}(\xi) \tag{16}$$

for $\xi \in [x_{j+\frac{1}{2}}, x_{j+\frac{1}{2}+n}]$. So the absolute value of the divided differences gives a measure of the smoothness of $W(x)$ in the interval.

The procedure to determine the smoothest support set is as follows. Define the stencil of $m + 1$ points, $S_m(j)$,

$$S_m(j) \equiv \{x_{j+\frac{1}{2}}, x_{j+3/2}, \ldots, x_{j+\frac{1}{2}+m}\} \tag{17}$$

Then for reconstruction on the interval $[x_{j-\frac{1}{2}}, x_{j+\frac{1}{2}}]$, set

$$i_1(j) = j \tag{18}$$

For higher order reconstruction, we determine the best cells by comparing the magnitudes of the divided differences. Consider adding a cell to the left and right of the current cell(s) and compare the corresponding two divided differences. We choose the smaller difference in magnitude to obtain the stencil that is smoothest in an asymptotic sense. Explicitly, identify

$$S_m^L \equiv S_m[i_{m-1}(j) - 1] \tag{19}$$

and

$$S_m^R \equiv S_m[i_{m-1}(j)] \tag{20}$$

Now build the stencil from its preceding stencil according to

$$\begin{aligned} i_m(j) &= i_{m-1}(j) - 1, \qquad \text{if } |W[S_m^L]| \le |W[S_m^R]| \\ &= i_{m-1}(j), \qquad \text{otherwise} \end{aligned} \tag{21}$$

The stencil is built for $m = 1, 2, 3, \ldots, n$.

Particularly note that the reconstruction does not pass through the cell centers in general but must satisfy conservation of the cell averages.

Reconstruction-via-Primitive ENO Scheme

The application of the ENO scheme to multidimensions is documented by Harten et al.[2] and Casper.[3] The two-dimensional ENO schemes based on the primitive function operate on data in one dimension at a time. Assume we have a Cartesian grid $j\text{dim} \times k\text{dim}$ in the (x, y) plane. Consider a reconstruction for the pointwise values of $w(x, y)$ on constant-x faces.

First, from a set of $j$dim cell averages (i.e., constant k row)

$$\bar{w}_{j,k} = \frac{1}{\Delta x_j} \int_{x_{j-\frac{1}{2}}}^{x_{j+\frac{1}{2}}} \frac{1}{\Delta y_k} \int_{y_{k-\frac{1}{2}}}^{y_{k+\frac{1}{2}}} w(x, y)\, dy\, dx \tag{22}$$

accurate line averages are reconstructed via the primitive function. This procedure is repeated for all $j$dim cells and all $k$dim rows. We then have a reconstruction for the line averages in the y direction

$$R(x; \bar{w}) = \frac{1}{\Delta y_k} \int_{y_{k-\frac{1}{2}}}^{y_{k+\frac{1}{2}}} w(x, y)\, dy \tag{23}$$

Another data set for reconstruction is generated by evaluating $R(x; \bar{w})$ at specific values of x, namely, at both vertical cell faces ($x = x_{j-\frac{1}{2}}^+, x_{j+\frac{1}{2}}^-$) for every cell. Then, with accurate line averages, pointwise data are obtained by a reconstruction in the y direction (i.e., with the reconstructed line averages $R(x_{j+\frac{1}{2}}^-; \bar{w})$, we obtain the pointwise reconstruction $R^2[y; R(x_{j+\frac{1}{2}}^-; \bar{w})]$, which is a polynomial in the y direction of degree k at the right face). Here the notation $x_{j+\frac{1}{2}}^-$ denotes the left state at $x_{j+\frac{1}{2}}$ and $x_{j-\frac{1}{2}}^+$ denotes the right state at $x_{j-\frac{1}{2}}$. R^2 is the pointwise reconstruction operating on R and is evaluated at the Gauss points of the flux integral. The notation at the left face, $x = x_{j-\frac{1}{2}}$, is then $R^2[y; R(x_{j-\frac{1}{2}}^+; \bar{w})]$. Two similar reconstructions are done for the constant-y faces. From these left and right states the flux integral can be accurately evaluated at the Gauss points with any flux-splitting technique.

Although notationally nasty, the reconstruction using line averages is crucial for arbitrary accuracy in two dimensions. For arbitrary three-dimensional accuracy, area averages, then line averages, and finally pointwise data must be reconstructed. The preceding ENO scheme logically chooses the smoothest stencil on each level from divided-difference tables of cell averages, area averages, and line averages in that order. The reconstruction satisfies the mean for all the cells in the support stencil and is of the form of a tensor-product polynomial, or more rigorously,

$$R(x, y, z, \bar{w}) = \sum_{i=0}^{k} \sum_{j=0}^{k} \sum_{l=0}^{k} c_{i,j,l}\, x^i y^j z^l \tag{24}$$

Note that for the reconstruction in two dimensions the ENO scheme will include $(k + 1)^2$ cells and in three dimensions $(k + 1)^3$ cells.

The previous reconstruction using the primitive function is applicable to stretched rectangular grids. However, a differentiable mapping from (x, y) space to (ξ, η) space is required for the extension to meshes with curvature. If the transformation is not known, this requires a polynomial of degree k passing through the grid points. The approximation to the pointwise function $w(x, y)$ in generalized coordinates is then

$$\tilde{w}(x, y) = \frac{R^2(x, y; A\bar{w})}{R^2(x, y; A)} \tag{25}$$

where $R^2(x, y; A\bar{w})$ and $R^2(x, y; A)$ are reconstructions for the pointwise functions $w(x, y)J(x, y)$ and $J(x, y)$, respectively. $J(x, y)$ is the transformation Jacobian from (x, y) space to (ξ, η) space.

$$A = \frac{1}{\Delta x \Delta y} \int J(x, y)\, dx\, dy \tag{26}$$

This formulation will maintain the freestream to the order of the truncation error in the finite-volume setting.

K-Exact Reconstruction

K-exact reconstruction is a simpler approach that makes no promises about the smoothness of the reconstructed solution. The method is multidimensional by nature and remains in the physical solution domain. The goal is simple: directly satisfy the mean for every cell in the stencil using the minimum number of cells necessary. K-exact reconstructions must satisfy three design criteria as specified by Barth and Frederickson[4]:

1) The reconstruction must satisfy conservation of the mean of the parent and support cells as in Eq. (3). If we consider a general polynomial $R(x, y, z; \bar{w})$,

$$R(x, y, z; \bar{w}) = \sum_{i=0}^{k} \sum_{j=0}^{k-i} \sum_{l=0}^{k-(i+j)} c_{i,j,l}\, x^i y^j z^l \tag{27}$$

then the reconstruction must satisfy the mean for $(k + 1)(k + 2)(k + 3)/6$ cells. For one- and two-dimensional polynomials, $k + 1$ and $(k + 1)(k + 2)/2$ cell means must be conserved, respectively. The support set must be in the neighborhood of the parent cell.

2) $R(x, y, z; \bar{w})$ must be k exact, which means that for polynomial functions $w(x, y, z)$ of degree k or less the reconstruction is exact.

3) The reconstruction process should be computationally efficient.

In contrast to the ENO reconstruction, the same k-exact reconstruction polynomial is used for all of the Gauss points on the cell's faces. Although the coefficients in $R(x, y, z; \bar{w})$ depend on the support stencil, the integral of $x^i y^j z^l$ depends only on the geometry of the grid cells. Applying the operation in Eq. (8), the mean of the reconstruction is

$$\bar{R}(x, y, z; \bar{w}) = \sum_{i=0}^{k} \sum_{j=0}^{k-i} \sum_{l=0}^{k-(i+j)} c_{i,j,l} \frac{1}{\Omega} \int_{\Omega} x^i y^j z^l \, d\Omega \tag{28}$$

The integral is strictly grid dependent whereas the coefficients are solution dependent. For the mth cell define the grid dependent integral as follows:

$$G_{i,j,l}(\Omega_m) \equiv \frac{1}{\Omega_m} x^i y^j z^l \, d\Omega \tag{29}$$

For a degree-k reconstruction, sufficient N [specifically, $(k+1)/2$] point Gauss quadrature integrates $G_{i,j,l}(\Omega_m)$ exactly. If the stencil never changes in the evolution of the solution, a fixed square matrix of $G_{i,j,l}(\Omega_m)$ can be decomposed into lower and upper triangular matrices prior to all of the time steps. Then, the system of equations for the coefficients $c_{i,j,l}$ can be solved by forward and backward substitution given a time level's cell averages. If the stencil should have to change from iteration to iteration as with ENO schemes, a lower/upper (LU) decomposition at every iteration would be required for a small matrix because the support set of Ω_m changes.

For the results of this paper, we choose the neighboring cells which deviate least from the parent cell based on a prescribed criteria. We choose only enough cells to ensure that the reconstruction is k exact. For the ith cell and all of the cells j in a search region in the neighborhood of i, determine

$$|\Delta \bar{w}_{i,j}| = |\bar{w}_i - \bar{w}_j| \tag{30}$$

Sorting $|\Delta \bar{w}_{i,j}|$ in increasing magnitudes yields a list from top to bottom of the best support cells for i. Then, the top k cells are used in the reconstruction provided the cells are contiguous. The symbol $\bar{w}$ in Eq. (30) may represent the spatial coordinates which would yield a support set of nearest neighboring cells for fixed-stencil algorithms. Likewise, $\bar{w}$ can represent the value of a fluid property such as density producing the smoothest stencil dependent upon the data. The stencil selection algorithm with $\bar{w}$ representing static pressure is used in the shock reflection problem to come. For all of the other applications, the stencil will be obtained using a nearest neighbor strategy where $\bar{w}$ represents the spatial coordinates.

A test must be applied to ensure the cells chosen are contiguous, or odd-even decoupling can occur. This can be seen in one dimension with a periodic hat function

$$\bar{w}_j = \begin{matrix} 1, & j \text{ even} \\ 0, & j \text{ odd} \end{matrix} \tag{31}$$

If the support cells are not contiguous by design, a reconstruction for cell i would use every other point and the hat function would satisfy the discrete wave equation in the steady state. A checkerboard function causes the same difficulty in two dimensions.

Dimensionally Split-Essentially Nonoscillatory Scheme

A one-dimensional reconstruction polynomial $R(x; \bar{w})$ has $k+1$ constants which are determined by satisfying conservation for $k+1$ cells in the stencil. Specifically, if the lowest cell number in a contiguous stencil of cells is i, then the reconstruction $R(x; \bar{w})$ must satisfy the cell averages of cells $i-i+k$.

For two-dimensional meshes we apply two such reconstructions to cell averages. The generated set of line averages is not further reduced to pointwise values as before, and subsequently, arbitrary accuracy is not achieved. The hope is to decrease CPU time of the ENO scheme while giving a better interpolation algorithm than the traditional fixed-stencil interpolations. Dimensionally split ENO accentuates physically real extrema and retains uniform high-order accuracy. The dimensionally split-ENO reconstruction may be summarized in formula as

$$R_{\mathrm{DS}}(x, y; \bar{w}) = R(x; \bar{w}) + R(y; \bar{w}) \tag{32}$$

For a rectangular grid the polynomial in the x direction $R(x; \bar{w})$ is applied to the vertical faces. Likewise, the polynomial in the y direction is applied to the horizontal cell faces.

ϕ-κ Reconstruction

The ϕ-κ formulation matches different cell averages for different combinations of ϕ and κ. For constant cell widths Δx and a local coordinate ξ zeroed at the center of cell j, the reconstruction which satisfies the mean of cells $j-1$ and j is

$$R_{-1}(\xi; \bar{w}) = \bar{w}_j + \left(\frac{\bar{w}_j - \bar{w}_{j-1}}{\Delta x} \right) \xi \tag{33}$$

The reconstruction which satisfies the mean of cells j and $j+1$ is

$$R_0(\xi; \bar{w}) = \bar{w}_j + \left(\frac{\bar{w}_{j+1} - \bar{w}_j}{\Delta x} \right) \xi \tag{34}$$

The traditional ϕ-κ formulation is a specific case of the reconstruction obtained by taking a linear combination of these two reconstructions and evaluating the result at $\xi = \Delta x/2$. A κ-dependent linear combination of the two reconstructions is

$$\begin{aligned} R(\xi; \bar{w}) &= \frac{(1-\kappa)}{2} R_{-1} + \frac{(1+\kappa)}{2} R_0 \\ &= \bar{w}_j + \frac{\xi}{2\Delta x} [(1+\kappa)\Delta + (1-\kappa)\nabla] \bar{w}_j \end{aligned} \tag{35}$$

The cell interface value of this reconstruction is the traditional ϕ-κ formulation

$$w_{j+1/2} = \bar{w}_j + (\phi/4)[(1+\kappa)\Delta + (1-\kappa)\nabla] \bar{w}_j \tag{36}$$

where ϕ is an on/off switch for higher order interpolation. Since three cell averages are used in the reconstruction, a third-order interpolation ($\kappa = 1/3$) can be obtained.

The underlying third-order reconstruction for the $\kappa = 1/3$ interpolation is obtained by satisfying conservation for the support set of cells $j-1$, j, and $j+1$. The unique third-order reconstruction that satisfies these cell averages is

$$\begin{aligned} R(\xi; \bar{w}) = \bar{w}_j &+ \frac{\bar{w}_j - \bar{w}_{j-1}}{\Delta x} \xi + \frac{\bar{w}_{j-1} - 2\bar{w}_j + \bar{w}_{j+1}}{2\Delta x^2} \\ &\times \left(\xi^2 + \xi \Delta x - \frac{\Delta x^2}{12} \right) - \frac{d^4 W}{dx^4} \frac{\Delta x^3}{2 \cdot 4!} \end{aligned} \tag{37}$$

This reconstruction is third order at all locations ξ. Specifically, this polynomial at the cell interface gives a third-order value $w_{j+1/2}$, which is identical to that obtained from the ϕ-κ formulation. This reconstruction step is often unrealized and should be utilized for correct high-order interpolations on nonuniform grids.

Merits and Deficiencies

The adaptive-stencil high-order accurate methods inherently will have poor high-frequency damping characteristics associated with the spatial differencing operator. A steady-state solution will only be possible if the time-evolution operator damps high-frequency noise. For a steady state, errors must

propagate from the domain and not return. Noise generation is constantly being reintroduced by the time-dependent chatter of the adaptive stencils. Even with perfectly absorbing boundary conditions, which would not reflect outgoing waves, the adaptive-stencil algorithms will constantly bring in truncation-error noise from the changing interpolations and prevent steady-state convergence to machine zero. For this reason, steady-state solutions obtained by convergence to machine zero and adaptive-stencil algorithms used to obtain arbitrarily high-order uniform accuracy are incompatible. We do not mean to convey that p refinement (increasing accuracy on the same mesh) gives worse solutions but merely that the sufficient number of iterations required to reflect a steady-state solution for a nonzero residual is not apparent. High-order uniformly accurate schemes lend themselves best to time-dependent problems where fluxes are inherently unbalanced. Typical residual histories for several steady-state problems are shown in Fig. 1. Notice that the Ringleb solutions are converged to machine zero because the monotonicity of the solution fixes the stencil for all time. The details of Ringleb's flow are further discussed in Sec. IV. Shu[8] and Atkins[9] have specifically addressed the issue of steady-state convergence by biasing the adaptive-selection algorithm to the more stable stencil.

Fixed-stencil algorithms do not suffer the same woes as do the moving-stencil algorithms in the march to a steady state. However, arbitrarily high-order accurate algorithms are not frequently coded in current production-level codes. The k-exact reconstruction method is by far the easiest to implement for general discretizations. All that is necessary is the precise flow domain and the inverted space matrix of polynomials to satisfy a mean quantity. We can control oscillations at discontinuities by either using a fixed-stencil algorithm, which constrains the accuracy yet attains steady-state convergence, or use a moving-stencil algorithm, which allows for arbitrarily high-order accuracy but does not achieve steady-state convergence in the sense of a machine-zero residual. A fixed-stencil algorithm is computationally much cheaper than its moving-stencil counterpart.

We investigate a simple compromise. A dimensionally split-ENO scheme will attain uniform accuracy but not arbitrary accuracy. Dimensionally split ENO hopefully requires less CPU time and recovers the time accuracy qualities of the moving-stencil algorithms, and the solution will still be essentially nonoscillatory. The time level for steady-state convergence will be questionable, and the strategy at boundaries is to limit the stencils in a TVD fashion. The results for this algorithm are given in Sec. IV.

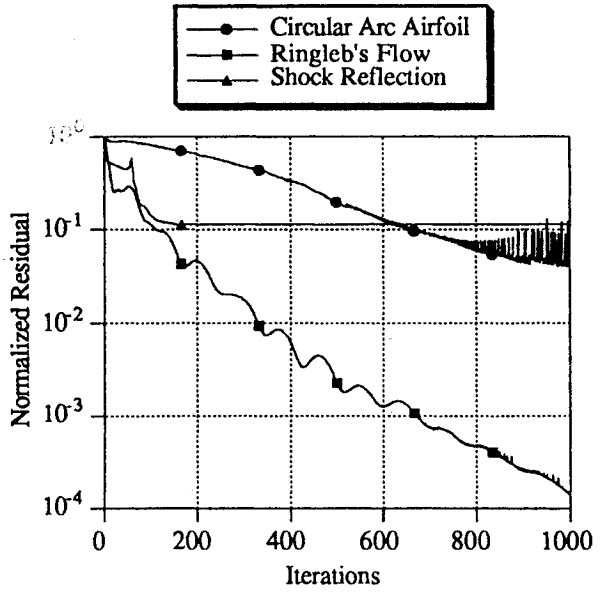

Fig. 1 Typical residual histories for problems using a chattering interpolation stencil.

III. Reconstruction Error

Consider the integral form of the heat equation with constant thermal properties

$$\frac{\mathrm{d}}{\mathrm{d}t}\int\int T(x, y)\,\mathrm{d}A + \oint \nabla T \cdot \hat{n}\,\mathrm{d}s = 0 \tag{38}$$

on the domain $I \in [0, 1] \times [0, 1]$ with the boundary conditions

$$T(x, 0) = T(x, 1) = T(0, y) = 0$$

and

$$T(1, y) = \sin(\pi y)$$

The exact solution under these constraints is

$$T(x, y) = \frac{\sinh(\pi x)\sin(\pi y)}{\sinh \pi} \tag{39}$$

We can measure the reconstruction error and numerical accuracy by calculating cell averages on several square grids and then reconstruct an approximation to $T(x, y)$. The L_p norm of the error in the temperature field is

$$\|\epsilon(x, y)\|_p \equiv = [\int |R(x, y; \bar{T}) - T(x, y)|^p\,\mathrm{d}A]^{1/p} \tag{40}$$

where $R(x, y; \bar{T})$ is a sufficiently accurate reconstruction using either the arbitrarily high-order accurate two-dimensional ENO scheme or the k-exact reconstruction. We compare degree-zero, degree-one, and degree-two reconstructions on several grids by evaluating the L_1 norm in Eq. (1) with four-point Gaussian quadrature for each cell. In general, the size of the problem domain must not change when refining the grid for accuracy-analysis studies. The slope of the L_p norm of the error vs Δx on a log-log plot is the accuracy r_c of the scheme. The computational accuracy is calculated in a discrete sense according to

$$r_c \equiv \frac{\log(\epsilon_{\Delta x_1}/\epsilon_{\Delta x_2})}{\log(\Delta x_1/\Delta x_2)} \tag{41}$$

Here, $\epsilon_{\Delta x_1}$ designates the norm of the temperature error on a grid with spacing Δx_1.

The reconstruction errors for the heat equation using the arbitrarily high-order accurate methods are plotted in Fig. 2. To interpret the results, consider the basis functions for the k-exact and two-dimensional ENO reconstruction operators. The ENO polynomial includes the first $(k + 1)^2$ set of basis polynomials, whereas the k-exact polynomial includes only enough to be k exact. A sample set of basis polynomials for $k = 2$ is shown in Fig. 3. The additional terms in the ENO polynomial and a search for the smoothest data set account for the lower reconstruction error with the RP-ENO method.

Operation counts for the high-order methods are given in Table 1 and Fig. 4. The operations for the RP-ENO scheme include calculating the difference tables consisting of characteristic variables, evaluating the high-order line averages, and determining the pointwise solution at the Gauss points. The k-exact scheme requires calculating the mesh averages, inversion of the left-hand matrix to determine the polynomial coefficients, and evaluating the reconstruction at the Gauss points. These two high-order methods require operations per grid cell of the same order. The benefit of dimensionally split ENO for this scalar reconstruction exercise is seen by a 10:1 decrease in the required number of operations. The DS-ENO scheme requires only the formation of the difference tables and one interface evaluation.

IV. Numerical Results

Ringleb's Flow

An exact compressible solution in the absence of shocks is necessary to measure the steady-state spatial accuracy of the

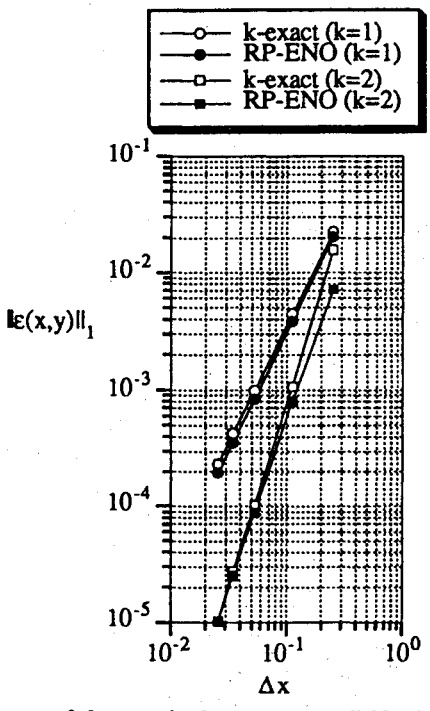

Fig. 2 L_1 norm of the error in the temperature field using RP-ENO and k-exact reconstruction error on the heat equation.

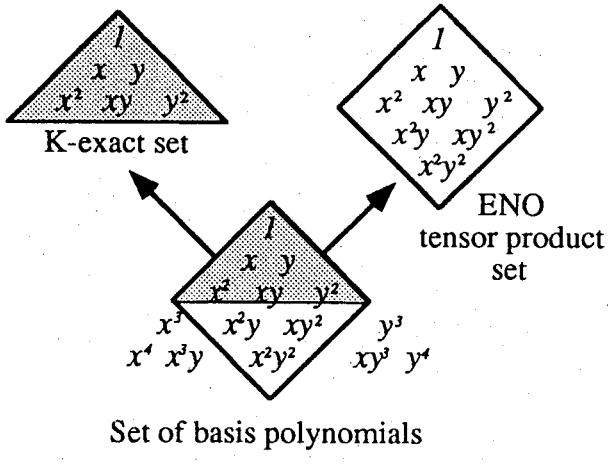

Fig. 3 Basis functions for two-dimensional ENO and k-exact reconstructions.

high accuracy schemes of this paper. Grid refinement on shocked solutions introduces higher frequencies on each successive grid which affects the numerical accuracy even away from discontinuities. Typically, researchers choose a model equation which is periodic in nature and has a known wave speed. The solution is traversed through several periods and compared with the exact solution at that time. We address the numerical error problem from a steady-state point of view. Assuming a solution can be converged to machine zero, a reconstruction of that steady-state solution can be compared with the exact solution to determine numerical error. For this purpose, we select the Ringleb flow documented by Chiocchia[10] and used for a similar purpose by Barth and Frederickson.[4]

Ringleb's flow is a transonic solution to the two-dimensional planar potential equation. Numerically, the Ringleb solution is obtained using k-exact and dimensionally split-ENO methods for degree-zero, degree-one, and degree-two reconstructions. Three grids of dimension 11×11, 21×21, and 41×41 are used with a streamline constant which varies from 1.47 on the left wall to 0.8 on the right wall. Figure 5 shows the 41×41 mesh.

Figure 6 shows degree-two pressure contours on the finest mesh with dimensionally split ENO. Flow moves from top left through the symmetric outflow on the bottom. Our domain is chosen so that the right wall is always subsonic while the left wall is transonic. The exact solution's contours would appear as nonconcentric circles for all flow variables.

Roe's approximate Riemann solver was used with the exact left and right states necessarily set on the inflow and outflow boundaries, respectively. The tangency boundary conditions on the left and right walls satisfy the normal-momentum equation

$$\frac{\partial p}{\partial n} = \frac{\rho(V \cdot V)}{R} \tag{42}$$

Table 1 Operations required per cell for reconstruction, with N the number of Gauss points and n the order of the interpolation

Scheme	Operations/grid cell
Two-dimensional RP-ENO	$(n-1)(n)(2n-1)^2/6 + 2[N+1](n-1)(n)(2n-1)/3 + [4N](n^2-1)$
Two-dimensional K exact	$(n)(n+1)(2n^3+n^2+11n)/4$
Two-dimensional DS-ENO	$(n-1)(n)(2n-1)/3 + 2(n^2-1)$
MUSCL	9

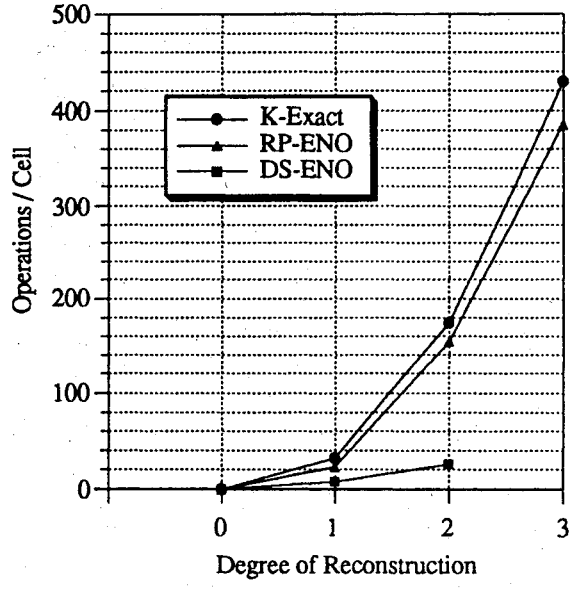

Fig. 4 Algorithm dependent operations required per cell for increasing accuracy.

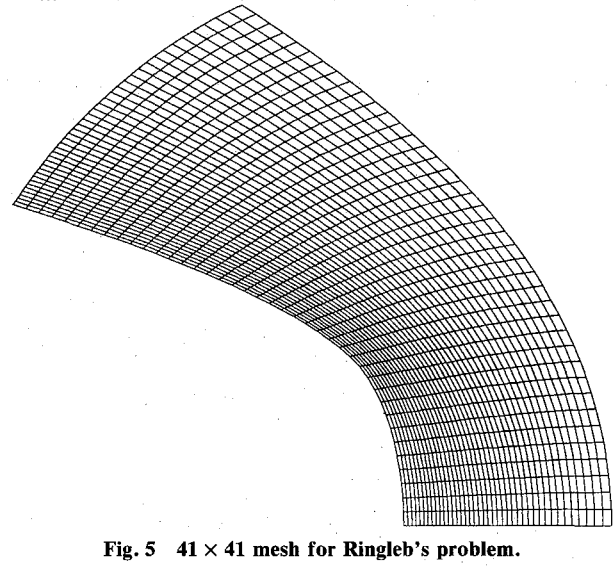

Fig. 5 41×41 mesh for Ringleb's problem.

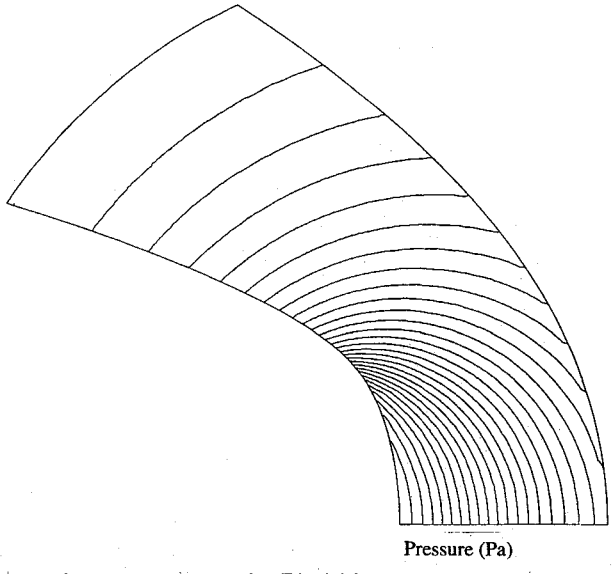

Fig. 6 Pressure contours for Ringleb's problem for a 41 × 41 grid using degree-two dimensionally split ENO.

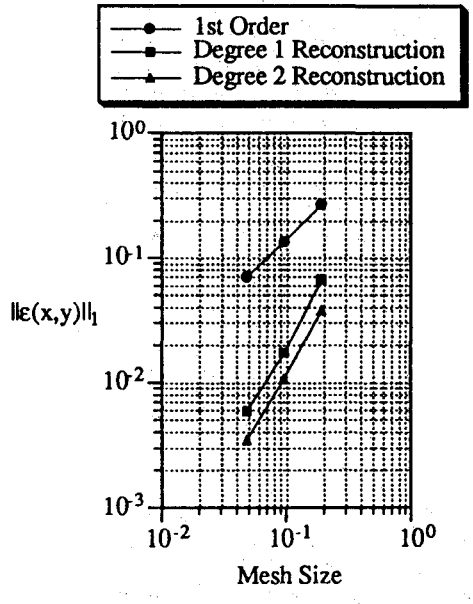

Fig. 7 Error in density field for Ringleb's problem with dimensionally split ENO.

where $\partial p/\partial n$ is the pressure gradient on the wall, ρ the density, V the velocity vector, and R the local radius of curvature. Note that R is negative for the right wall and positive for the left wall. The pressure gradient was evaluated to the accuracy of the interior-point scheme.

The L_2 norm of the density error is shown in Fig. 7 for the DS-ENO scheme and in Fig. 8 for the k-exact scheme. As is expected, the dimensionally split-ENO scheme will achieve no better than second-order accuracy; however, the numerical-solution error for $k = 2$ is less than the error for $k = 1$. The k-exact scheme attains computational accuracies of 0.986, 2.15, and 2.92 for degree-zero, degree-one, and degree-two reconstructions, respectively.

Shock Reflection

A simple inviscid flow is used as a test case for preliminary calculations for the dimensionally split-ENO scheme and the k-exact reconstruction algorithms. A simple Cartesian grid is used to simulate a $M_\infty = 2.9$ oblique shock with a wave angle $\beta = 29$ deg reflecting off of a flat surface. A grid of 61×31 was used with constant spacing in both directions. Particular attention was given to how our stencil choice algorithm would maneuver through the shock-shock interactions on the surface.

The ENO scheme assumes adequately smooth data is available in some direction. The logic in the scheme itself chooses that smoothest direction to build the reconstruction. Obviously, when discontinuities are close to boundaries, the underlying assumption of a smooth data set breaks down. For the shock reflection, all of the boundary interpolations were forced to the interior. The resulting oscillations were expected

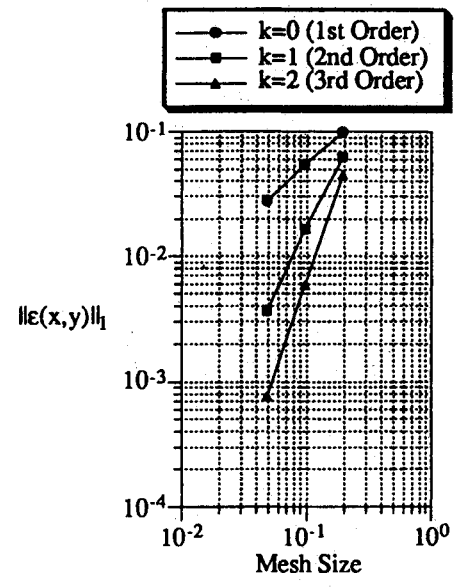

Fig. 8 Error in density field for Ringleb's problem with k-exact reconstruction.

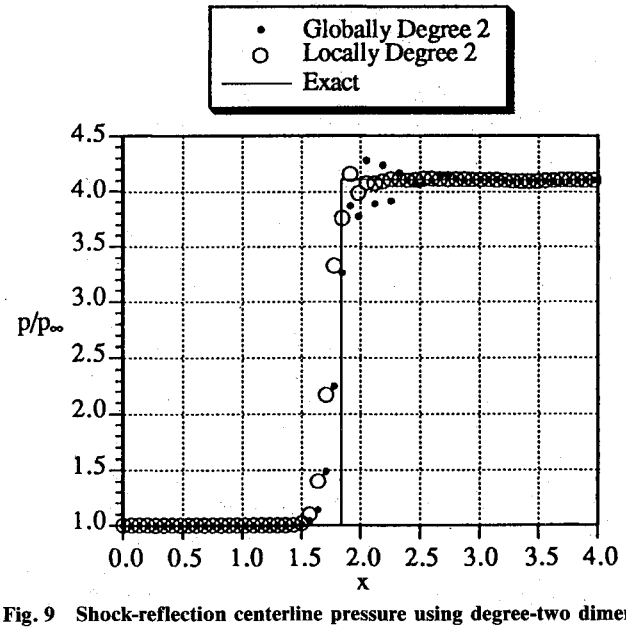

Fig. 9 Shock-reflection centerline pressure using degree-two dimensionally split ENO.

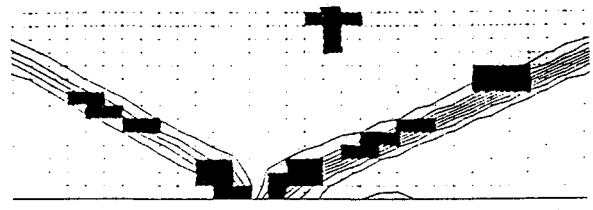

Fig. 10 Stencils selected for the shock reflection with k-exact reconstruction.

and controlled with a reduction of accuracy at cells where the norm of the subset characteristic variable difference table increased in magnitude. Figure 9 shows the centerline pressure with and without reduction in accuracy using the dimensionally split-ENO scheme with $k = 2$.

The multidimensional reconstruction step used in the k-exact method allows the stencil to adjust with the shock thus introducing little or no oscillations as compared to dimensionally split ENO. Figure 10 focuses on the stencils selected near the shock reflection point and demonstrates the effectiveness of the simple stencil selection algorithm. Overshoots are very limited and effectively controlled. Approximately 99 and 84% of the stencils were not changing after the shock had developed for the cases of $k = 1$ and $k = 2$, respectively. The LU is frozen for these stencils, and the computational effort is greatly reduced.

Vortex-Shock Interaction

The propagation of a wake vortex through a normal shock is investigated and compared to the experimental results of Naumann and Hermanns[11] and the numerical results of Meadows et al.[12] and Casper.[13] The flow depicts two main fluid phenomena: a secondary sound wave that propagates from the initial interaction position and a spreading angle of this sound wave. The strength of the secondary wave and the spreading angle depend on the strength of the shock and the strength of the vortex, respectively. The interferogram at 58 μs after the vortex strikes the shock is shown in Fig. 11.

To numerically simulate this interaction, the steady-state expansion through a 1/2-deg diverging section is calculated with a standing shock at the midsection. The vortex model of Meadows et al.[13] is then superimposed onto the velocity field, and the time evolution evaluated according to the Shu and Osher[14] TVD Runge-Kutta scheme with third-order temporal accuracy. Density contours are shown on the 101×121 mesh at 101.1 μs after the superposition in Fig. 12. Quantitative results show improvement over the second-order results of Meadows et al.[12] and more dissipation than the true high-order accurate results of Casper.[13]

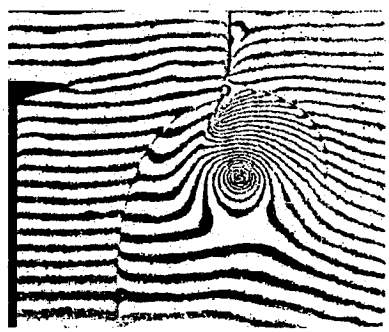

Fig. 11 Interferogram of vortex-shock interaction showing the secondary wave and spreading angle.

V. Conclusions

An essentially nonoscillatory (ENO) scheme is described which will achieve at best second-order accuracy in two and three dimensions but is an order of magnitude cheaper than the full reconstruction-via-primitive (RP) ENO and k-exact schemes. Results for the Ringleb flow verify this result. A method to choose the best support stencil locally for the k-exact reconstruction is robust and possesses the oscillation control qualities of ENO. Results for a shock reflection show the ability of our choice of algorithm to avoid interpolation across a shock that impinges with a boundary surface. The ENO scheme must be modified to control the interpolation and subsequent oscillations in this shock-wall region. Reconstruction error on the heat equation shows the truncation error realized by each scheme. Finally, a vortex-shock interaction shows the ability of the ENO scheme to excel in capturing high-frequency physical phenomenon in a time-accurate setting. Steady-state convergence will inevitably be unattainable with a chattering stencil which introduces a different local truncation error in magnitude, not order, at each time step. Practical application of the k-exact scheme will depend on the ability to quickly solve small systems of equations for the polynomial coefficients. The ENO schemes and k-exact schemes will inevitably produce successful results for time-dependent flows.

Acknowledgments

This work was sponsored under NASA Grant NAG-1-776 and McDonnell-Douglas Grant 91-0185-07.

References

[1]Harten, A., and Osher, S., "Uniformly High-Order Accurate Essentially Non-Oscillatory Schemes I," *SIAM Journal of Numerical Analysis,* Vol. 24, No. 2, 1987, pp. 279–309.

[2]Harten, A., Engquist, B., Osher, S., and Chakravarthy, S. R., "Uniformly High-Order Accurate Essentially Non-Oscillatory Schemes III," *Journal of Computational Physics,* Vol. 71, 1987, pp. 231–323.

[3]Casper, J., "An Extension of Essentially Non-Oscillatory Shock Capturing Schemes to Multi-Dimensional Systems of Conservation Laws," Ph.D. Dissertation, Old Dominion Univ., Dec. 1930.

[4]Barth, T. J., and Frederickson, P. O., "Higher Order Solution of the Euler Equations on Unstructured Grids Using Quadratic Reconstruction," AIAA Paper 90-0013, Reno, NV, Jan. 1990.

[5]Abgrall, R., "Design of an Essentially Non-Oscillatory Reconstruction Procedure on Finite-Element Type Meshes," NASA CR 189574 and Institute for Computer Applications in Science and Engineering Rept. 91-84, Langley Research Center, Dec. 1991.

[6]Chakravarthy, S. R., "Some Aspects of Essentially Non-Oscilla-

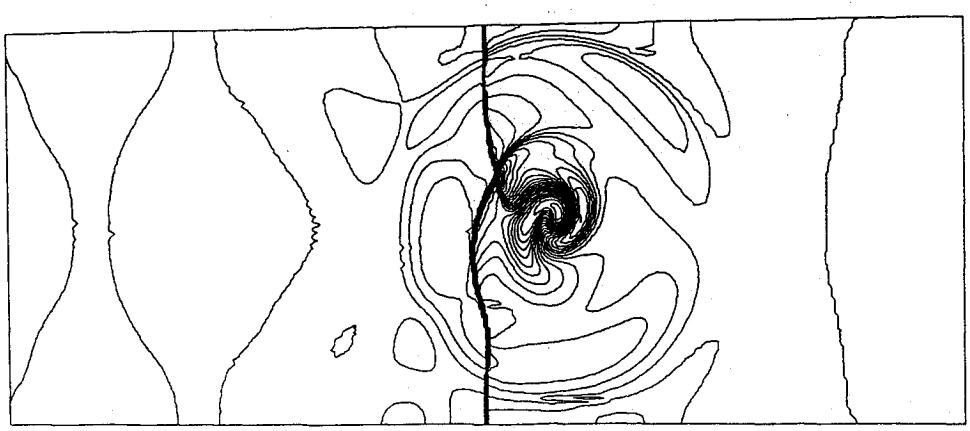

Fig. 12 Density contours for vortex-shock interaction at 101.1 μs using degree-two dimensionally split ENO.

tory (ENO) Formulations for the Euler Equations," NASA CR 4285, May 1990.

[7]Harten, A., "Short Course: Numerical Methods for Hyperbolic Conservation Laws," Institute for Computer Applications in Science and Engineering Internal Rept., Document 33., Nov. 25, 1986.

[8]Shu, C.-W., *Journal of Scientific Computing,* 1990.

[9]Atkins, H., AIAA Paper 91-1557, Honolulu, HI, Jan. 1991.

[10]Chiocchia, G., "Exact Solutions to Transonic and Supersonic Flows," AGARD Advisory Rept. AR-211, Sept. 1985.

[11]Naumann, A., and Hermanns, E., "On the Interaction Between a Shock Wave and a Vortex Field," AGARD-CP-131, 1973.

[12]Meadows, K., Kumar, A., and Hussaini, M., "A Computational Study on the Interaction Between a Vortex and a Shock Wave," AIAA Paper 89-1043, San Antonio, TX, April 1989.

[13]Casper, J., "Finite Volume Application of High Order ENO Schemes to Two-Dimensional Boundary Value Problems," AIAA Paper 91-0631, Reno, NV, Jan. 1991.

[14]Shu, C.-W., and Osher, S., "Efficient Implementation of Essentially Non-Oscillatory Schemes," *Journal of Computational Physics,* Vol. 77, 1988, pp. 439–471.